Chemical Engineering Science 107 (2014) 311–316

Contents lists available at ScienceDirect

Chemical Engineering Science

journal homepage: www.elsevier.com/locate/ces

Porosity variation below a fluid–porous interface

Arzhang Khalili [a,b,*], Mohammad Reza Morad [c], Maciej Matyka [d], Bo Liu [a], Reza Malekmohammadi [a], Jörg Weise [e], Marcel M.M. Kuypers [a]

[a] Max Planck Institute for Marine Microbiology, Bremen, Germany
[b] Jacobs University Bremen, Bremen, Germany
[c] Sharif University of Technology, Tehran, Iran
[d] Institute for Theoretical Physics, University of Wrocław, Wrocław, Poland
[e] Fraunhofer Institute for Manufacturing Technology and Advanced Materials, Bremen, Germany

HIGHLIGHTS

- Derivation of a depth-dependent porosity relation below a fluid–porous interface.
- Assumption is based on spheres, randomly packed as a porous medium.
- Validation of relation by non-invasive laser method and numerical simulations.
- Comparison of the results with literature data on biofilm porosity.
- Showing effect of variable porosity on solute concentration profile in a biofilm.

ARTICLE INFO

Article history:
Received 15 August 2013
Received in revised form
5 December 2013
Accepted 17 December 2013
Available online 27 December 2013

Keywords:
Microbial mat
Biofilm
Porous interface
Variable porosity
Sphere packing

ABSTRACT

The correct quantification of porosity is essential in all studies pertaining to porous media. A host of existing works employs a constant, bulk value for porosity, even when the porous sample is attached to a free fluid. Since the volume fraction of the solid matrix near the interface region differs from that in the core, the porosity undergoes a spatial variation. Here we present a novel relation for the porosity as a function of depth below the interface, using the concept of surface roughness applied on the classical definition of open porosity. This relation has been verified by computational modeling as well as non-invasive laser experiments. It has been shown that this depth-dependent porosity relation applies also to a non-granular porous layer such as a biofilm.

1. Introduction

Porosity has been known to be the most significant property describing a porous medium. Moreover, its correct quantification is essential for flow, heat and mass transfer parameters such as permeability, tortuosity, thermal conductivity and diffusion coefficient.

In a variety of situations, a porous medium has a boundary with its non-porous surrounding such as a free fluid. Examples include microbial mats (Wieland et al., 2001), biofilms (Lewandowski, 2000), Rayleigh–Benard convection in fluid permeating a porous medium (Howle et al., 1993), monochromatic surface waves across fluid–porous interfaces (Albers, 2006), air-grain flows in granular media (Sandnes et al., 2010). In such cases, the porosity undergoes a spatial decrease due to increase of solid matrix density or packing density with depth. This fact has been already pointed out in previous studies (Ochoa-Tapia and Whitaker, 1995; Goyeau et al., 2003; Goharzadeh et al., 2005), however, a functional relationship for the depth-dependent porosity at fluid–porous interfaces has remained illusive.

Here we present a novel porosity–depth relation by applying the classical definition of open porosity to each thin slice of the porous layer below the fluid–porous interface. This relation is found to be applicable to granular as well as naturally growing porous layers.

To validate this relation, rigorous experimental and numerical investigations were performed. The experiments were composed of non-invasive planar laser induced fluorescence (PLIF) technique to visualize void and solid fractions below the interface. Solid matrix was considered to be mono-sized spherical glass beads.

* Corresponding author at: Max Planck Institute for Marine Microbiology, Bremen, Germany.
E-mail address: akhalili@mpi-bremen.de (A. Khalili).

0009-2509/$ - see front matter © 2014 Published by Elsevier Ltd.
http://dx.doi.org/10.1016/j.ces.2013.12.021

In the numerical approach, a free surface of randomly packed solid spheres was first generated. The porous layer underneath the free surface was then split into thin slices which were used to extract void and solid matrix fractions. Both experimental and numerical results agreed well with the porosity–depth relation presented.

Finally, the significance of inclusion of a depth-dependent porosity has been demonstrated on the example of oxygen concentration profile predicted for a biofilm.

2. Development of a new porosity–depth relation

We consider a cubic container of volume L^3 filled with a random packing of Nsmall solid spheres of diameter d having an interface with the overlaying fluid layer. Following previous studies (Beavers and Joseph, 1967; Neale and Nader, 1974; Goharzadeh et al., 2005) the position of the nominal fluid–porous interface, $y=0$, is defined as the location of the horizontal tangent to the perimeter of the uppermost sphere (Fig. 1). We introduce a transition layer with the thickness δ understood as the layer within which the porosity falls from unity at the fluid–porous interface to its bulk value in the porous core. To calculate the depth-dependent porosity, the transition layer is divided into an ensemble of M subsequent tiny horizontal slices of thickness, $\Delta = L/N$, occupied partially by fluid and partially by solid segments (top image in Fig. 1). The open porosity of each tiny horizontal slice can be given by

$$\varphi_m = 1 - \frac{1}{L^2 \Delta} \sum_{i=1}^{p} V_i \tag{1}$$

where V_i is the volume of each sphere segment and p is the total number of segments in a given slice m. The sum in Eq. (1) generally represents a trapezoidal volume similar to the so-called Tower of Hanoi (Buneman and Levy, 1980; Wolfram, 2011). It can be shown (see results section) that in a random packing of large number of spheres, the thickness Δ corresponds to the vertical distance which separates any two vertically closest spheres. With other words at a given depth there would exist only one sphere and the trapezoidal volume fades to the volume of a spherical cap $V(y)$ (right image in Fig. 1). Consequently, Eq. (1) converts to

$$\varphi(y) = 1 - \frac{N}{L^3} V(y) \tag{2}$$

with

$$V(y) = \pi d^3 \left[\frac{1}{2} \left(\frac{y}{d} \right)^2 - \frac{1}{3} \left(\frac{y}{d} \right)^3 \right]. \tag{3}$$

We recall that the volume fraction of solid spheres to the container volume can be given by

$$1 - \varphi_b = \frac{N \frac{\pi d^3}{6}}{L^3}. \tag{4}$$

Hence, upon substitution of Eq. (3) in Eq. (2) and elimination of N/L^3 from Eq. (2) using Eq. (4), one obtains the depth-dependent porosity relation as

$$\varphi(y^*) = 1 - (1 - \varphi_b) \left[3y^{*2} - 2y^{*3} \right]. \tag{5}$$

Here φ_b represents bulk porosity and $y^* = y/d$. The term $1-\varphi_b$ provides a universal constant which ranges from 0.609 to 0.641 for poured and close random packing (Dullien, 1992). The above relation has been derived under the premise that the solid spheres are randomly packed, provide point of contact with their neighboring ones, generate interconnected voids and are heavier than the saturating fluid.

3. Numerical and experimental methods

3.1. Numerical determination of porosity variation

To generate a random packing of N mono-sized spherical solid beads in a given cubic box of size L, a standard algorithm developed in Princeton University has been utilized (Skoge et al., 2006; Princeton, 2011). The Princeton code has been modified by us to construct a porous layer with a free interface with the fluid on top. To do so, we numerically remove the beads from the top of the box until we reach those beads with their centers below $y=0$ as shown in Fig. 2.

The constructed porous layer has the thickness $L/2+d/2$. Knowing the exact coordinates of the solid beads and voids, the porosity of each horizontal cross-sectional stripe of thickness Δ – representing the porosity at a given depth – is given by $\phi_i = A_{void} \cdot \Delta / A_{total} \cdot \Delta$. Hence, at any given depth the porosity can be extracted from the void to total area fraction. The repetition of this procedure for the entire whole porous layer leads to a numerically driven depth-dependent porosity relation.

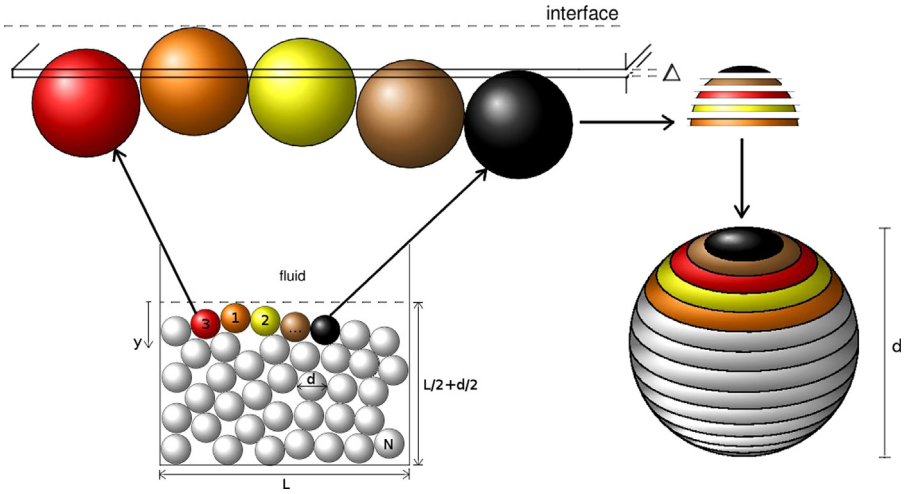

Fig. 1. A porous layer of solid spheres having a free interface with the upper fluid layer (bottom left image); any, sufficiently tiny, horizontal slice of thickness Δ (top image) will be occupied partially by solid and partially by void or fluid. Porosity at any depth is related to the volume of the segments confined within Δ constructing a spherical cap (bottom right image).

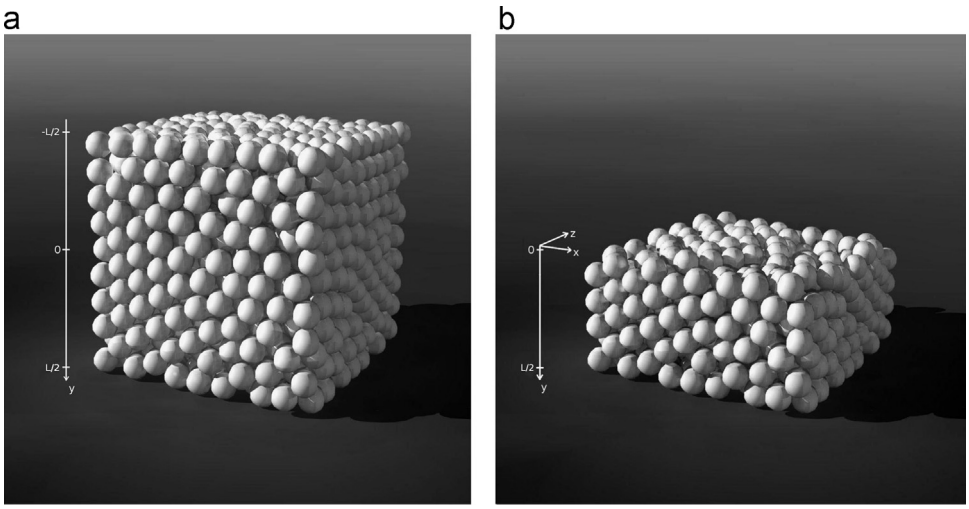

Fig. 2. The random sphere packing created with the numerical code (Skoge et al., 2006). In the example shown here, the system initially consisted of $N=1000$ spheres (image a), from which approximately half were removed to generate a free, porous interface with the fluid-only layer above (image b).

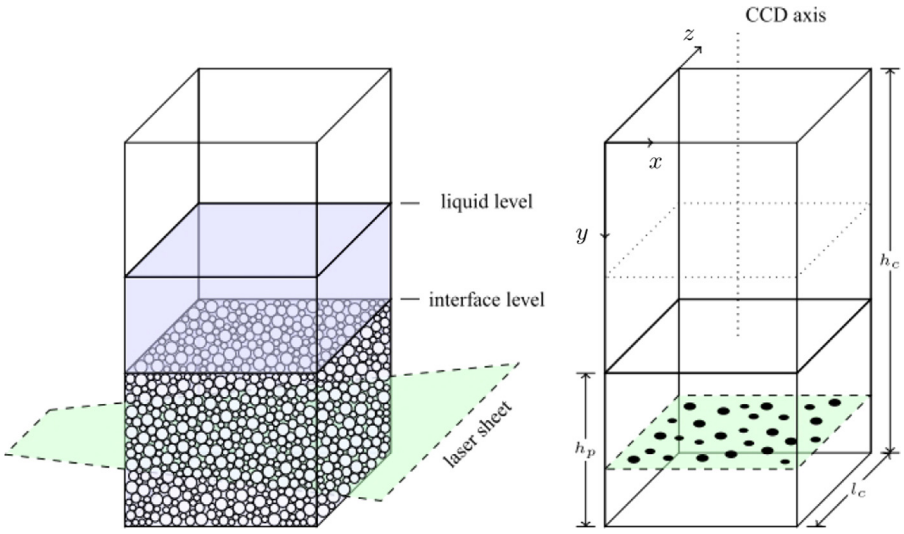

Fig. 3. Schematics of the setup for the glass beads experiments. After matching the refractive indices of the fluid and glass beads, the laser light (green plane in the left image) can illuminate the entire container cross section, in which the void areas can be differentiated from the solid ones (right image). Black circles denote cross sections of intersected spheres. (For interpretation of the references to color in this figure caption, the reader is referred to the web version of this paper.)

3.2. Experimental determination of porosity variation

The porosity variation has been measured using the PLIF technique as described in the following manner. A 200 mm high transparent rectangular container with a cross section area of 96×96 mm^2 was filled with Duran^{TM} glass beads of diameter 6.5 mm to the height of 75 mm (Fig. 3). The packing was saturated with a mixture of Dow Corning silicon oils DC 550 and DC 556 with a volume fraction of 29% and 71%, respectively, leading to an optimal refractive index match between the glass beads and the fluid ($n=1.471$). A continuous-wave Nd-YAG laser (Laser Quantum Ventus, 532 nm, 1.5 W) was used to illuminate a horizontal cross section (green plane in figure) with a wavelength suitable for the absorption band of the dye (500–600 nm). As dye, Nile Red 20 μg/l was applied. Using a CCD camera (PCO 1600) mounted on top of the container the entire cross section (void and solid areas) was captured. The rectangular container has been mounted on a linear positioning system with a resolution of 10 μm to adjust its vertical position with respect to the horizontal laser sheet. The laser sheet was located above the free surface (porosity equal 1). The container was elevated until the first evidence of the uppermost sphere appeared in the image as a black dot. This position was experimentally considered as the interface for the corresponding system. Then, the container was elevated at constant increments of 0.5 mm to acquire depth-dependent images for porosity determination.

The 2D images were digitalized using the Matlab image analysis tool with standard algorithm. Briefly speaking, the algorithm consists of the following steps: (i) applying a median filter for removal of small granular artefacts, (ii) adjusting the contrast, (iii) subtracting background light from each image, and finally (iv) constructing binary images, in which the void and solid areas are digitalized. The porosity as a function of depth was obtained in the same manner discussed above.

The details of the samples taken in the computational and laboratory experiments are summarized in Table 1.

4. Results and discussion

An optimal random sphere packing is reached when only one sphere center ordinate is found at a given depth (Skoge et al.,

Table 1
Sample specifications used in numerical and experimental setups.

Sample	Generation mode	Material	d	N
I	Numerical	Solid sphere	0.1/0.05/0.023/0.0183	$10^3/10^4/10^5/2\times10^5$
II	Experimental	Spherical glass beads	6.5 mm	2961

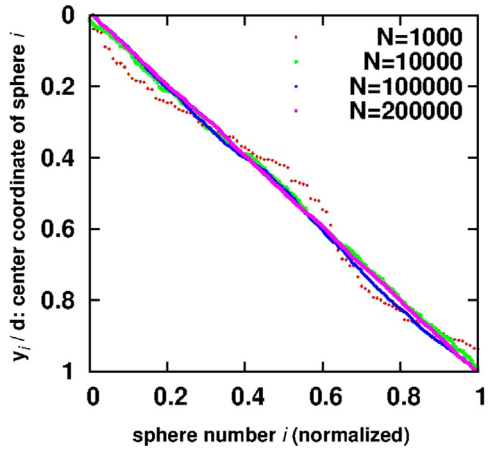

Fig. 4. Sphere center ordinate as a function of the sphere number. The perfect linear trend represented by N=100000 indicates the fact that the center ordinate of each sphere is vertically shifted with respect to all others, i.e. one sphere center at a given depth.

2006). To find the sufficient number of solid spheres ensuring this goal, N has been stepwise increased as $N=10^3$, 10^4, 10^5 and 2×10^5. As depicted in Fig. 4 a good linear distribution of sphere center depth coordinate versus sphere number has been reached already by $N=100\,000$. However, to be on the secure side, for all computations performed in this study N was set up to 200 000. With this N the dimensionless diameter of each solid sphere would read as $d=0.0183$.

In Fig. 5 the results of the numerical (first row) and experimental (second row) investigations are summarized. The images in the first three columns refer to cross-sections at different depths below the interface. From each image one can obtain the porosity at the given depth. The differently sized black circles in each image indicate the intersected spheres at the corresponding depth. Starting from the interface ($y=0$) and analyzing the cross-section images we reach to a depth, below which no more changes in the porosity can be observed, yielding the thickness of the transition layer δ.

In the experiments with the glass beads the transition layer thickness amounted to $\delta\approx6.5$ mm which is equal to the diameter (d) of the glass beads used. Similarly, the dimensionless transition layer thicknesses in the numerical simulations were $\delta\approx0.1$, 0.05, 0.023 and 0.0183, equivalent to the dimensionless diameter of generated solid spheres. Hence, it can be deduced that transition layer thickness correlates well with the diameter of the grain size used. This finding confirms the predictions of Goharzadeh et al. (2005). The diagrams in the fourth column of Fig. 5 show the numerically and experimentally determined porosity variation (symbols) versus the analytical prediction from Eq. (5) (solid line). The latter corresponds to the right ordinate, while the former refers to the left ordinate. Obviously, the analytical prediction best describes the porosity variation within the transition layer and could be used as a standard relation when the solid matrix is composed of mono-sized spheres.

With Eq. (5) at hand, it is worth examining whether or not this relation could be applied to non-granular porous layers. To do this, we take the biofilm studies of Lewandowski (2000) and Zhang and Bishop (1994a, 1994b). Using micro-slicing technique, these authors have characterized spatial distribution of biofilm properties such as porosity. The data pertinent to the porosity–depth of these studies have been plotted in Fig. 6 along with the ones predicted by Eq. (5). Note that the meaning of y^* in Eq. (5) for the biofilm is y/δ in which δ represents the transition layer thickness. The good agreement between predicted and the published, experimental porosity profiles underlines the applicability of our finding to the porosity variation within a biofilm. The reason for this agreement can be based on the following fact. As mentioned earlier, the optimal number of solid spheres ensuring the best results was found to be $N=200\,000$. Therefore, it is plausible to assume that such a large random configuration of spheres with a thin transition layer resembles well with the fluffy layers and random nature of a biofilm. Because the porosity–depth relation did not alter significantly upon increase of N up to 200 000, the relation can be regarded as valid for biofilm too.

At this point, it is interesting to see the effect of porosity variation on the interfacial mass and heat transfer phenomena. As an example, we take the diffusion of a solute from a fluid layer into a biofilm with a constant sink. Following Beyenal and Lewandowski (2005) the one-dimensional, steady-state diffusion-reaction in the biofilm can be expressed as

$$\frac{\partial}{\partial y^*}\left(\frac{1}{T^2}\frac{\partial C^*}{\partial y}\right)=(1-\varphi)\frac{V_m^*C^*}{K_m^*+C^*}. \tag{6}$$

The dimensionless quantities C^*, y^*, V_m^* and K_m^* denote concentration, depth, rate constant and saturation constant, respectively, and are normalized with $C^*=C/C_0$, $y^*=y/\delta$, $V_m^*=V_m\delta^2/D_0C_0$ and $K_m^*=K_m/C_0$ in which C_0 is the concentration at the surface of the biofilm and D_0 is the free solution diffusion coefficient. Furthermore, T represents the tortuosity and is given by $T^2=1-0.77\ln\varphi$ (Matyka et al., 2008). The corresponding boundary conditions were set as $C=1$ and $\partial C/\partial y=0$ at the surface and bottom of the biofilm, respectively. The parameters were taken as $K_m^*=0.1$ and $V_m^*=1$ from the pertinent literature (Beyenal and Lewandowski, 2005).

It should be noted that by Eq. (6) the biofilm has been treated as a continuum with averaged physical properties at each depth. One may also consider the biofilm as a porous medium and perform an averaging procedure similar to that carried out by Valdés-Parada et al. (2006, 2007).

Obviously, the choice of porosity, a constant or a depth-dependent one, will have a direct influence on the concentration distribution obtained from Eq. (6) within the transition layer. This difference has been demonstrated in Fig. 7.The predictions show that concentration profiles are significantly different and the solute penetrates much deeper into the biofilm when taking porosity variation into account. A similar trend has been also reported for homogeneous and stratified biofilm by Beyenal and Lewandowski (2005).

Finally, a note should be made to the classical study of Carman et al. (1937) in which he derived the relation:

$$\varphi=1-\frac{4\sqrt{2}}{3}\left(\frac{d}{D}\right)^2 \tag{7}$$

for the bulk porosity of pairwise staggered spheres (of diameter d) placed in a tetrahedron arrangement inside a cylindrical tube of

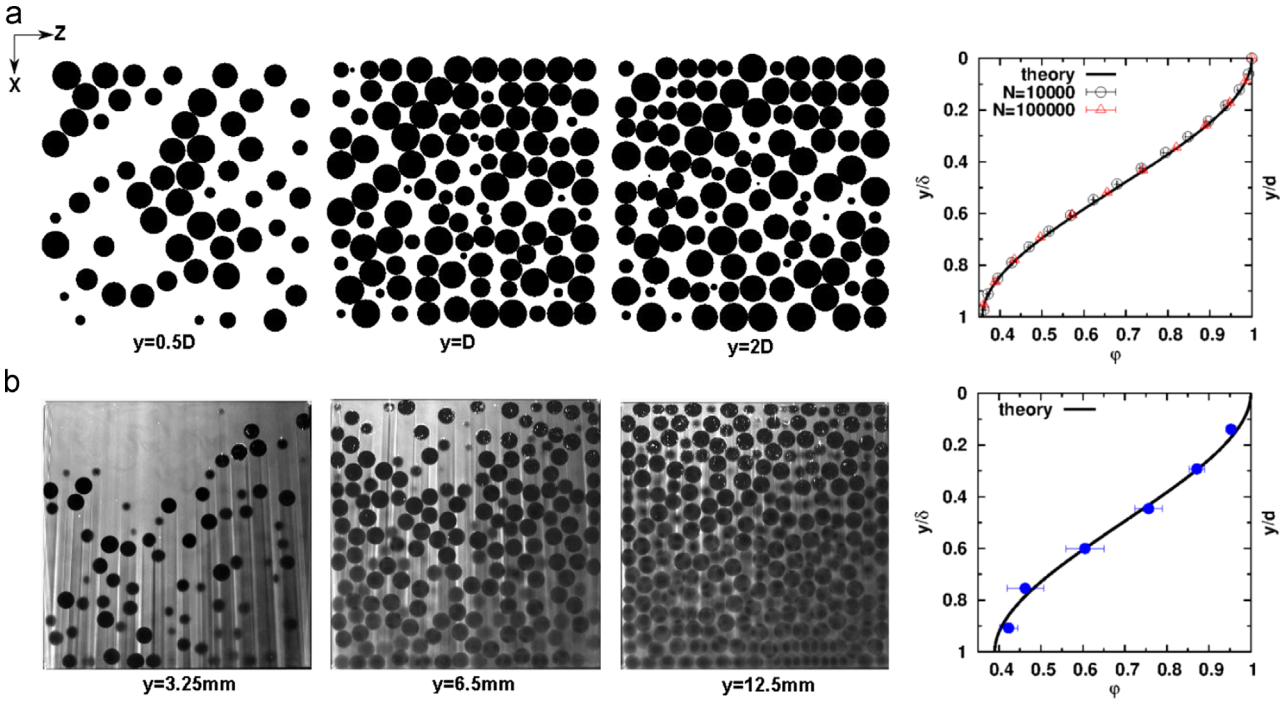

Fig. 5. Numerically packed spheres: (a) the differently sized circles indicate the intersected spheres at different depths; (b) same for lab experiments with glass beads; images in the right column show the porosity as a function of depth within the transition layer. Solid lines denote the trend predicted by Eq. (5) while symbols refer to computer and lab experiments.

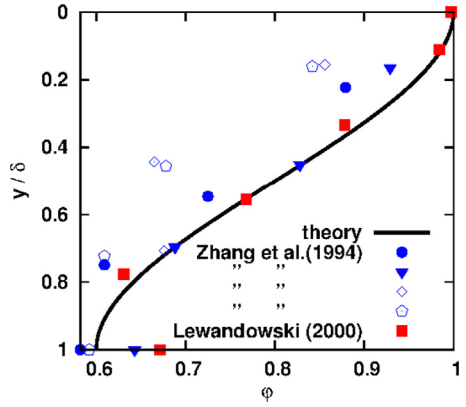

Fig. 6. Comparison of depth-dependent porosity predicted from Eq. (5) (solid line) with experimental porosity measurements within a biofilm (symbols). The filled red square symbols are from Lewandowski (2000) while the others are taken from Zhang and Bishop (1994a, 1994b). Here, δ represents the transition layer thickness of the biofilm. (For interpretation of the references to color in this figure caption, the reader is referred to the web version of this paper.)

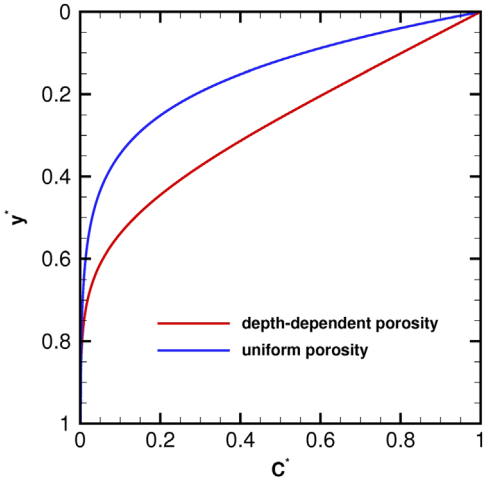

Fig. 7. Concentration profiles predicted with uniform porosity and depth-dependent porosity.

diameter D. He simplified his relation to $\varphi = 0.528$ for $D/d = 2$. This value can also be obtained as a special case of Eq. (2) when taking $N=2$, $L^3 = h\pi D^2/4$, and $V = \pi D^3/6$, leading to $\varphi = 0.529$ for the porosity of a cylindrical segment of height h (compare with Fig. 8, cf. Carman et al., 1937).

5. Conclusions

We derived analytically a porosity–depth relation below the interface between a porous layer and a clear fluid on top. To verify the relation, we performed numerical and laboratory experiments. In the numerical part a porous layer was constructed by random packing of mono-sized spheres with a free interface. By knowing the exact coordinate of the spheres and voids, the porosity of each three dimensional horizontal stripe of infinitesimal thickness was calculated for different depths. In the experimental part, a non-invasive planar laser induced fluorescence technique was used to visualize void and solid fractions within the aforementioned three dimensional stripes. Both data sets obtained from numerical and experimental investigations agreed well with those predicted by the analytical relation. Next, we showed that this relation may even be applied to describe the porosity variation in non-granular porous layers such as biofilms. Furthermore, the impact of depth-dependent porosity was exemplified by the diffusion of a solute from a fluid layer into a porous layer underneath with a constant sink. Finally, we showed that the classical study of Carman for the porosity of pairwise staggered spheres in a tetrahedron arrangement can be derived as a special case of the porosity–depth relation introduced in this study.

Acknowledgments

This work was supported by the Max Planck Society (MPG). We thank the Dow Corning Chemicals for providing the silicon oils for free. We acknowledge Zbigniew Koza and Dietrich Stoyan for reading the manuscript and Zbigniew Lewandowski for the discussions of biofilms. We also thank Salvatore Torquato for his comments on the paper and bringing into our attention the discussion about sphere packing ambiguity. A.K. thanks Versorgungsamt Bremen for providing the work assistance.

References

Albers, B., 2006. Monochromatic surface waves at the interface between poroelastic and fluid halfspaces. Proc. R. Soc. A 462 (2067), 701–723.
Beavers, G.S., Joseph, D.D., 1967. Boundary condition at a naturally permeable wall. J. Fluid Mech. 30, 197–207.
Beyenal, H., Lewandowski, Z., 2005. Modelling mass transport and microbial activity in stratified biofilms. Chem. Eng. Sci. 60, 4337–4348.
Buneman, P., Levy, L., 1980. The towers of Hanoi problem. Inf. Process. Lett. 10 (4–5), 243–244, http://dx.doi.org/10.1016/0020-0190(80)90150-7, ISSN 0020-0190, URL ⟨http://www.sciencedirect.com/science/article/pii/0020019080901507⟩.
Carman, P.C., 1937. Fluid flow through granular beds. Trans. Inst. Chem. Eng. 15, 150–166.
Dullien, F.A.L., 1992. Porous Media: Fluid Transport and Pore Structure. Academic Press, San Diego.
Goharzadeh, A., Khalili, A., Jørgensen, B.B., 2005. Transition layer thickness at a fluid-porous interface. Phys. Fluids 17 (057102), 1–10.
Goyeau, B., Lhuillier, D., Gobin, D., Velarde, M.G., 2003. Momentum transport at a fluid-porous interface. Int. J. Heat Mass Transf. 46, 4071–4081.
Howle, L.E., Behringer, R.P., Georgiadis, J.G., 1993. Visualization of convective fluid flow in a porous medium. Nature 362, 230–232.
Lewandowski, Z., 2000. Notes on biofilm porosity. Water Res. 34 (9), 2620–2624.
Matyka, M., Khalili, A., Koza, Z., 2008. Tortuosity–porosity relation in porous media flow. Phys. Rev. E, 78, 026306.
Neale, G., Nader, W., 1974. Practical significance of Brinkman′s extension of Darcy′s law: coupled parallel flows within a channel and a bounding porous medium. Can. J. Chem. Eng. 52, 475–478.
Ochoa-Tapia, J.A., Whitaker, S., 1995. Momentum transfer at the boundary between a porous medium and a homogeneous fluid—II. Comparison with experiment. Int. J. Heat Mass Transf. 38, 2647–2655.
Princeton, 2011, http://cherrypit.princeton.edu/Packing/C++/.
Sandnes, B., Flekkøy, E.G., Knudsen, H.A., Måløy, K.J., See, H., 2010. Patterns and flow in frictional fluid dynamics. Nat. Commun. 2 (288).
Skoge, M., Donev, A., Stillinger, F.H., Torquato, S., 2006. Packing hyperspheres in high-dimensional Euclidean spaces. Phys. Rev. E 74 (4), 041127, http://dx.doi.org/10.1103/PhysRevE.74.041127.
Valdés-Parada, F., Goyeau, B., Ochoa-Tapia, A., 2006. Diffusive mass transfer between a microporous medium and an homogeneous fluid: jump boundary conditions. Chem. Eng. Sci. 61, 1692–1704.
Valdés-Parada, F., Goyeau, B., Ochoa-Tapia, A., 2007. Jump momentum boundary condition at a fluid-porous dividing surface: derivation of the closure problem. Chem. Eng. Sci. 62, 4025–4039.
Wieland, A., de Beer, D., Damgaard, L.R., Kühl, M., van Dusschoten, D., Van As, H., 2001. Fine-scale measurement of diffusivity in a microbial mat with nuclear magnetic resonance imaging. Limnol. Oceangr. 46, 248–259.
Wolfram, 2011. ⟨http://mathworld.wolfram.com/TowerofHanoi.html⟩.
Zhang, T., Bishop, P., 1994a. Density, porosity, and pore structure of biofilms. Water Res. 28 (11), 2267–2277.
Zhang, T., Bishop, P., 1994b. Evaluation of tortuosity factors and effective diffusivities in biofilms. Water Res. 28 (11), 2279–2287.